Analytical investigation on the buckling and free vibration of porous laminated FG-CNTRC plates

Tahir Ghazoul[a], *Mohamed Atif* Benatta[b],
Abdelwahhab Khatir[c], *Youcef* Beldjelili[d],
Baghdad Krour[e], *Mohamed* Bachir Bouiadjra[f]

[a] University of Djillali Liabes, Structures and Advanced Materials
in Civil Engineering and Public Works Laboratory,
Sidi Bel Abbes, People's Democratic Republic of Algeria,
e-mail: tahir.ghazoul@univ-sba.dz, **corresponding author**,
ORCID iD: https://orcid.org/0009-0006-9869-4339

[b] University of Djillali Liabes, Structures and Advanced Materials
in Civil Engineering and Public Works Laboratory,
Sidi Bel Abbes, People's Democratic Republic of Algeria,
e-mail: bematif@gmail.com,
ORCID iD: https://orcid.org/0009-0007-5854-9054

[c] Polytechnic University of Marche, Structural Section DICEA,
Ancona, Italian Republic,
e-mail: a.khatir@pm.univpm.it,
ORCID iD: https://orcid.org/0000-0003-4920-5165

[d] University of Djillali Liabes, Structures and Advanced Materials
in Civil Engineering and Public Works Laboratory,
Sidi Bel Abbes, People's Democratic Republic of Algeria,
e-mail: beldjelili.youcef@gmail.com,
ORCID iD: https://orcid.org/0000-0003-3877-9665

[e] University of Djillali Liabes, Structures and Advanced Materials
in Civil Engineering and Public Works Laboratory,
Sidi Bel Abbes, People's Democratic Republic of Algeria,
e-mail: baghdad.krour@univ-sba.dz,
ORCID iD: https://orcid.org/0000-0002-8265-9807

[f] University of Djillali Liabes, Structures and Advanced Materials
in Civil Engineering and Public Works Laboratory,
Sidi Bel Abbes, People's Democratic Republic of Algeria;
Thematic Agency for Research in Science and Technology,
Algiers, People's Democratic Republic of Algeria,
e-mail: mohamedbachirbouiadjra@gmail.com,
ORCID iD: https://orcid.org/0009-0008-4814-6187

Abstract:

Introduction/purpose: The aim of this study is to examine the buckling and free vibration behavior of laminated composite plates reinforced with carbon

nanotubes when various sources of uncertainty are taken into account with the main focus being the existence of porosity.

Methods: A porous laminated plate model is developed using a high order shear deformation theory. Different configurations of functionally graded aligned single-walled carbon nanotubes throughout the thickness of each layer are being investigated. The effective properties of materials are evaluated through the extended rule of mixture while considering an upper bound for the effect of porosity. The governing equations are derived and solved using the virtual work principle and Navier's approach. The validity of the current formulation is confirmed by comparing the results with the existing data from literature sources. The impact of numerous parameters such as porosity, carbon nanotube volume fraction, reinforcement distribution types, lamination scheme, and the number of layers on the buckling and free vibration responses is investigated in detail.

Results: A key finding of this study is the significant reduction in buckling resistance of laminated FG-CNTRC plates due to porosity, contrasting with the minor impact on the free vibration response.

Conclusion: The results of this paper emphasize the critical role of porosity in structural integrity and provide novel insights into the behaviour of advanced composite materials.

Key words: buckling, free vibration, laminated composite plate, porosity, functionally graded material, carbon nanotubes.

Introduction

Carbon nanotubes (CNTs) are recognized as excellent reinforcements for advanced composites owing to their superior properties and low density. In contemporary industries such as aeronautical, mechanical and civil engineering, these advanced composite materials integrated in the form of shells, plates or beams as structural components have found significant applications. As required, the accurate evaluation of the mechanical reactions of structures fabricated from CNTs reinforced composite materials (CNTRC) becomes crucial for engineering design and manufacture.

Over recent years, significant attention has been devoted by researchers to functionally graded CNTRC materials (FG-CNTRC) featuring spatially varying characteristics based on a specific non-uniform distribution of the reinforcement phase. The discovery of this interesting feature led to different studies on the mechanics of CNTRC structures. Shen (2009) has introduced the first study on FG-CNTRC. His findings suggested that functionally graded reinforcement might increase the bending moment. According to Kwon et al. (2011), FG-CNTRC can be

achieved utilizing a powder metallurgy manufacturing method with a non-uniform dispersion of CNTs throughout the layer. The bending and free vibration of different kinds of FG-CNTRC plates were investigated by Zhu et al. (2012). They discover that reinforcements distributed near the bottom and top are more effective than those dispersed close to the mid-plane in enhancing the stiffness of CNTRC plates. Lei et al. (2013) used the element-free kp-Ritz method to study the buckling of FG-CNTRC plates. They found that for all different distributions of CNTs, those closer to the bottom and top exhibit larger buckling load values contrasted with other types of reinforcement arrangements. Liew et al. (2015) conducted a comprehensible review of the existing literature encompassing static, buckling, dynamic and non-linear analyses of FG-CNTRC.

On the other hand, researchers assert that multi-layered composite structures offer superior mechanical performance compared to single-layer structures. Laminated composite plates are highly attractive for structural applications due to their exceptional weight-to-stiffness ratio and the capacity to tailor the lamination scheme to meet specific design requirements. In conjunction with the expansion application of laminated composites in engineering structures, numerous deformation plate theories have been developed to precisely forecast their behavior. Kirchhoff (1850) developed the simplest theory, known as the classical plate theory (CLPT); however, it is not applicable to thick plates as it ignores completely the effects of shear deformation. Mindlin (1951) proposed the first-order shear deformation plate theory (FSDT) which considers shear deformation effects and is applicable to both thin and moderately thick plates. Nevertheless, the FSDT requires the use of a shear correction factor to meet zero shear conditions on the surfaces of the plate. Determining the correct value of this factor is challenging, which is considered a shortcoming of the FSDT. Later, higher-order shear deformation theories (HSDT) were developed (Reddy, 1984; Shimpi et al, 2003; Mantari et al, 2012) to overcome the limitations of the FSDT. These theories avoid the need for shear correction factors by assuming non-linear stress variation through the thickness. Subsequently, researchers arrived at a class of the refined plate theory (RPT) by disassembling transverse displacements into bending and shear components (Thai & Choi, 2011; Thai & Vo, 2013). The HSDT is often desirable for its superior accuracy over the CLPT and the FSDT. However, HSDTs with five or six variables are even more accurate for analyzing laminated composite plates than RPTs. Sayyad & Ghugal (2015) provided a synthesis of recent research conducted on multi-layered composite plates that utilized various shear deformation theories.

1244

Stimulated by the concept of FG-CNTRC and the benefits of multi-layered composite structures, researchers have been inspired to study FG-CNTRC multi-layered structures. This approach has the advantage of arranging the CNTs where the reinforcement is most effective and the ability to orient them in such a way as to obtain the highest mechanical properties from the laminated composite structures. Malekzadeh & Shojaee (2013) examined the buckling of CNTRC quadrilateral laminated plates using the FSDT. Zhang & Selim (2017) incorporated Reddy's HSDT for free vibration analyses of FG-CNTRC thick laminated plates. Lei et al. (2018) used the CLPT combined with the element-free method to analyse the vibration behavior of matrix-cracked hybrid (FG-CNT/conventional fiber) laminated composite plates. Alimoradzadeh et al. (2023) analysed the thermo-mechanical buckling of FG-Fiber laminated composite beams using the Euler-Bernoulli beam theory. Chiker et al. (2023) investigated how the uncertainty caused by the non-ideal aligned distribution of FG-CNTs nano-fillers affects the free vibration characteristics of laminated FG-CNTRC plates. Fu et al. (2019) introduced a model based on the nth-order shear deformation theory to conduct static analysis of FG-CNTRC laminated plates supported by elastic foundations under thermal conditions. Arani et al. (2021) used Reddy's shear deformation theory to analyze the forced and free vibrations of FG-CNTRC laminated cylindrical panels. Tran et al. (2020) devised a novel four-variable RPT to perform static analysis on smart FG-CNTRC laminated plates incorporating a piezoelectric actuator and subjected to electro-mechanical loads. Daikh et al. (2023) analyzed the static bending response of composite laminated beams reinforced with randomly oriented FG-CNTs and fiber reinforcements on an elastic foundation, employing the finite element method. An analytical model for examining the free vibration of thick laminated plates reinforced with FG-graphene composites was introduced by Ma & Jin (2023).

However, perfection remains elusive, and fiber composite materials are no exception. During their manufacturing, there are many imperfections that are created. These imperfections exert a considerable influence on the mechanical characteristics of composite materials, often causing them to deviate from expected values. Thoughtfully planned and tightly controlled manufacturing processes can decrease the occurrence of defects, thereby enhancing material properties, albeit typically resulting in increased costs (Ciriscioli et al, 1991). This would change if one could evaluate and quantify the effect of defects and, based on that, allow a certain level of defects in composite materials parts as a means to estimate the quality of a composite. In this way, the desired properties and safety

factors can be achieved at a lower cost and with reduced manufacturing energy.

As a result of its importance in fiber composite materials, porosity stands out as the most extensively studied manufacturing defect. In modern composite materials, removing pores has become increasingly challenging, due to a higher complexity of parts and the heightened viscosity of modified polymers (Lee et al, 2006). Mehdikhani et al. (2019) conducted a review on porosity in fiber composite materials, including its formation, characteristics, and effects.

The literature contains a considerable amount of research on the impact of porosity on the inter-laminar shear strength of Fiber/epoxy composites (Hernández et al, 2011; Stamopoulos et al, 2016; Hayashi & Takahashi, 2017). Others are keen on assessing how porosity affects the physical and mechanical characteristics of unidirectional fiber plant composites (Madsen & Lilholt, 2003; Madsen et al, 2009). However, studies focusing on the effect of porosity on CNTRCs are rare, particularly concerning the analysis of their mechanical responses. Guessas et al. (2018) analytically studied the impact of matrix porosity on the buckling response of a CNTRC porous plate via FSDT considering a semi-empirical approach established by Phani & Niyogi (1987) describing the relationship between porosity and Young's modulus in brittle solids. Medani et al. (2019) employed identical assumptions to study the static and dynamic behavior of an FG-CNTRC porous sandwich plate. In their studies, it was found that porosity has an undeniable effect on the mechanical responses of CNTRC structures.

From the aforementioned review, it is clear that a limited number of studies have been conducted to analyze the structural responses of CNTRCs with porosities. The literature currently available also indicates that multi-layered FG-CNTRC structures have captured the interest of numerous researchers, not only because of their intricate construction, but also because they pose challenges.

The current study focuses on developing an analytical model to analyze the buckling and free vibration performance of laminated FG-CNTRC plates while accounting for the presence of porosity. The extended rule of mixture is formulated to assess the effective material properties of the resulting nanocomposites in the presence of porosity, taking into account an upper limit for its influence. Four different distribution types of CNTs along the thickness of the layers are being examined, encompassing uniform distribution as well as three other functionally graded distributions. The adopted shear deformation theory ensures the appropriate distribution of transverse shear strains throughout the

thickness and imposes tangential stress-free boundary conditions on the surfaces. The governing equations are derived through the virtual work principle and solved using Navier's solutions. The results obtained by the present method are compared with the results from the existing literature. Detailed parametric analyses are performed to investigate the influences of porosity, CNTs distributions, CNTs volume fraction, the number of layers, CNTs fiber orientation, stacking sequence and aspect ratio on the buckling and free vibration characteristics of porous laminated FG-CNTRC plates.

Theoretical formulations

Effective material properties

Consider a rectangular plate with the total thickness h, the length a and the width b, composed of N perfectly bonded layers, with reference to the coordinate system depicted in Figure 1.

The component layers are presumed to consist of a blend of single-walled CNTs (SWCNTs) and an isotropic matrix. In consideration, there are four different types of CNT distribution throughout the layer thickness: uniform distribution (UD) and functionally graded distributions denoted by FG-O, FG-V and FG-X.
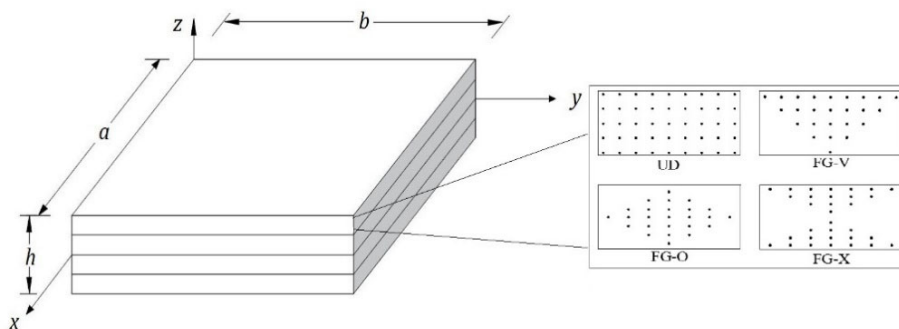

Figure 1 – Different configurations of CNTs through the layer thickness

As a result, the volume fraction of CNTs can be expressed based on their configuration throughout the thickness of each individual layer as:

$$V_{CNT} = \begin{cases} V_{CNT}^* & UD \\[2mm] \left(1+\dfrac{2z}{h}\right)V_{CNT}^* & FG\text{-}V \\[3mm] 2\left(1-\dfrac{2|z|}{h}\right)V_{CNT}^* & FG\text{-}O \\[3mm] 2\left(\dfrac{2|z|}{h}\right)V_{CNT}^* & FG\text{-}X \end{cases} \tag{1}$$

where

$$V_{CNT}^* = \frac{W_{CNT}}{W_{CNT} + (\rho^{CNT}/\rho^m) - (\rho^{CNT}/\rho^m)W_{CNT}} \tag{2}$$

W_{CNT} is the mass fraction of CNTs, ρ^{CNT} and ρ^m are the densities of the CNTs and the matrix, respectively. V_{CNT} and V_{CNT}^* are the volume fractions of CNTs for UD and FG-CNTRC, respectively.

It is assumed that the mass volume of CNTs in the UD-CNTRC layer and the FG-CNTRC layers is the same, meaning: $V_{CNT} = V_{CNT}^*$.

The extended rule of mixture, as a straightforward and convenient micromechanics model, is used to determine the effective material properties of the CNTRC layer (Shen, 2009):

$$E_1 = \eta_1 V_{CNT} E_1^{CNT} + V_m E^m \tag{3a}$$

$$\frac{\eta_2}{E_2} = \frac{V_{CNT}}{E_2^{CNT}} + \frac{V_m}{E^m} \tag{3b}$$

$$\frac{\eta_3}{G_{12}} = \frac{V_{CNT}}{G_{12}^{CNT}} + \frac{V_m}{G^m} \tag{3c}$$

where E_1^{CNT} and E_2^{CNT} are the Young's moduli of CNTs in longitudinal and transverse directions, respectively, and G_{12} is the shear modulus. G_{12}^{CNT} is the shear modulus of CNTs, E^m and G^m are the Young's modulus and shear modulus of the matrix. η_1, η_2 and η_3 are the efficiency parameters which serve to account for load transfer between CNTs and the polymeric matrix. V_{CNT} and V_m are CNTs and matrix volume fractions which satisfy the relation:

$$V_{CNT} + V_m = 1 \tag{4}$$

In the previous study, Hagstrand et al. (2005) theoretically and experimentally investigated how void content affects the structural flexural performance of unidirectional glass fiber reinforced polypropylene composite. Consequently, they set an upper threshold for the impact of void content on the composite elastic modulus using the relationship:

$$E(v_{void}) = E_0(1 - v_{void})$$ (5)

where $E(v_{void})$ and E_0 represent the elastic modulus in the presence and absence of voids, respectively. v_{void} represents the void volume fraction.

Similarly, the effective elastic moduli of the CNTRC in equation (3) as a function of porosity can be derived as follows:

$$E_i^P = E_i(1 - P), i = 1, 2, 12$$ (6)

where P represents the volume fraction of porosity and E_i^P is the effective elastic modulus in the presence of porosity.

As Poisson's ratio exhibits weak dependence on the position, it is assumed that v_{12} remains constant across the thickness of CNTRC plates:

$$v_{12} = V_{CNT} v_{12}^{CNT} + V_m v^m$$ (7)

where v_{12}^{CNT} and v^m are the Poisson's ratios of CNTs and the matrix, respectively.

Density ρ as a function of porosity is given by:

$$\rho = V_{CNT} \rho^{CNT} + (V_m - P)\rho^m$$ (8)

where ρ^{CNT} and ρ^m are the density of CNTs and the matrix, respectively.

Kinematics equations

According to the theory of material point situated at (x, y, t) in the plate domain, the displacements field can be formulated as follows:

$$u(x, y, z, t) = u_0(x, y, t) - z.w_{,x} + f(z)\phi_x$$ (9a)

$$v(x, y, z, t) = v_0(x, y, t) - z.w_{,y} + f(z)\phi_y$$ (9b)

$$w(x, y, z, t) = w_0(x, y, t)$$ (9c)

Here u, v and w represent the displacements in the x, y and z directions, respectively. u_0, v_0 and w_0 denote mid-plane displacements, while ϕ_x and ϕ_y denote shear rotations. All generalized displacements are the functions of x, y and time t. $f(z)$ denotes the shape function governing the

transverse shear strain and stress distribution across the thickness. In terms of HSDTs, it is defined as (Sayyad & Ghugal, 2015):

$$f(z) = z - \frac{4}{3}\left(\frac{z^3}{h^2}\right) \qquad (10)$$

It is crucial to note that, depending on the selected shape function, the displacement field in (9) can be readily adjusted to fit other plate theories. For instance, the CLPT is achieved by using the zero shape function while the FSDT is obtained with $f(z) = z$. From the theory of small deformations, the non-zero strain components related to the displacement field in (9) are defined as follows:

$$\begin{Bmatrix} \varepsilon_x \\ \varepsilon_y \\ \gamma_{xy} \end{Bmatrix} = \begin{Bmatrix} u_{0,x} \\ v_{0,y} \\ u_{0,y} + v_{0,x} \end{Bmatrix} + z \begin{Bmatrix} -w_{0,xx} \\ -w_{0,yy} \\ -2w_{0,xy} \end{Bmatrix} + f(z) \begin{Bmatrix} \phi_{x,x} \\ \phi_{y,y} \\ \phi_{x,y} + \phi_{y,x} \end{Bmatrix} ; \begin{Bmatrix} \gamma_{yz} \\ \gamma_{xz} \end{Bmatrix} = f'(z) \begin{Bmatrix} \phi_y \\ \phi_x \end{Bmatrix} \quad (11)$$

with

$$f'(z) = \frac{df(z)}{dz} \qquad (12)$$

Constitutive relations

Given that the plate consists of multiple orthotropic layers, the stress state within each layer is expressed as:

$$\begin{Bmatrix} \sigma_x \\ \sigma_y \\ \sigma_{xy} \\ \sigma_{yz} \\ \sigma_{xz} \end{Bmatrix}^k = \begin{bmatrix} \bar{Q}_{11} & \bar{Q}_{12} & \bar{Q}_{16} & 0 & 0 \\ \bar{Q}_{12} & \bar{Q}_{22} & \bar{Q}_{26} & 0 & 0 \\ \bar{Q}_{16} & \bar{Q}_{26} & \bar{Q}_{66} & 0 & 0 \\ 0 & 0 & 0 & \bar{Q}_{44} & \bar{Q}_{45} \\ 0 & 0 & 0 & \bar{Q}_{45} & \bar{Q}_{55} \end{bmatrix}^k \begin{Bmatrix} \varepsilon_x \\ \varepsilon_y \\ \gamma_{xy} \\ \gamma_{yz} \\ \gamma_{xz} \end{Bmatrix} \qquad (13)$$

where $\{\sigma\}^k$; $\{\varepsilon\}$ and $\left[\bar{Q}_{ij}\right]^k$ are the stress vector, the strain vector and the transformed stiffness matrix, respectively.

The components of the transformed stiffness matrix $\left[\bar{Q}_{ij}\right]^k$ are defined as follows:

$$\bar{Q}_{11}^k = Q_{11}^k \cos\theta + 2\left(Q_{12}^k + 2Q_{66}^k\right)\cos^2\theta\sin^2\theta + Q_{22}^k \sin^4\theta;$$
$$\bar{Q}_{12}^k = \left(Q_{11}^k + Q_{22}^k - 4Q_{66}^k\right)\cos^2\theta\sin^2\theta + Q_{12}^k\left(\sin^4\theta + \cos^4\theta\right);$$
$$\bar{Q}_{22}^k = Q_{11}^k \sin^4\theta + 2\left(Q_{12}^k + 2Q_{66}^k\right)\cos^2\theta\sin^2\theta + Q_{22}^k \cos^4\theta;$$
$$Q_{16}^k = \left(Q_{11}^k - Q_{12}^k - 2Q_{66}^k\right)\cos^3\theta\sin\theta + \left(Q_{12}^k - Q_{22}^k + 2Q_{66}^k\right)\sin^3\theta\cos\theta;$$
$$\bar{Q}_{26}^k = \left(Q_{11}^k - Q_{12}^k - 2Q_{66}^k\right)\cos\theta\sin^3\theta + \left(Q_{12}^k - Q_{22}^k + 2Q_{66}^k\right)\sin\theta\cos^3\theta; \qquad (14)$$
$$\bar{Q}_{66}^k = \left(Q_{11}^k + Q_{22}^k - 2Q_{12}^k - 2Q_{66}^k\right)\cos^2\theta\sin^2\theta + Q_{66}^k\left(\sin^4\theta + \cos^4\theta\right);$$
$$\bar{Q}_{44}^k = Q_{44}^k \cos^2\theta + Q_{55}^k \sin^2\theta;$$
$$\bar{Q}_{45}^k = \left(Q_{55}^k - Q_{44}^k\right)\cos\theta\sin\theta;$$
$$\bar{Q}_{55}^k = Q_{55}^k \cos^2\theta + Q_{44}^k \sin^2\theta;$$

where θ is the angle formed by the global plate coordinate and the individual layer's local material coordinate. Q_{ij}^k are the plane stress-reduced stiffnesses expressed in terms of the engineering constants along the material axes of the layer as follows:

$$Q_{11}^k = \frac{E_{11}}{1-v_{12}v_{21}}; Q_{12}^k = \frac{v_{12}E_{22}}{1-v_{12}v_{21}}; Q_{22}^k = \frac{E_{22}}{1-v_{12}v_{21}}; Q_{66}^k = G_{12}; Q_{44}^k = G_{23}; Q_{55}^k = G_{13} \qquad (15)$$

Equations of motion

The governing equations are derived here using the virtual work principle. The principle can be expressed analytically as:

$$\int_{t1}^{t2} \delta\left(U_P + V - T\right) dt = 0 \qquad (16)$$

The strain energy of the plate is computed by:

$$\delta U_P = \int_V \left[\sigma_x \delta\varepsilon_x + \sigma_y \delta\varepsilon_y + \sigma_{xy}\delta\gamma_{xy} + \sigma_{yz}\delta\gamma_{yz} + \sigma_{xz}\delta\gamma_{xz}\right] dxdydz \qquad (17)$$

$$\delta U_P = \int_A \begin{bmatrix} N_x\delta u_{0,x} + N_y\delta v_{0,y} + N_{xy}(\delta u_{0,y} + \delta v_{0,x}) - \\ M_x^w\delta w_{0,xx} - M_y^w\delta w_{0,yy} - 2M_{xy}^w\delta w_{0,xy} + \\ M_x^f\delta\phi_{x,x} + M_y^f\delta\phi_{y,y} + M_{xy}^f(\delta\phi_{x,y} + \delta\phi_{y,x}) + \\ Q_{yz}\delta\phi_y + Q_{xz}\delta\phi_x \end{bmatrix} dxdy \qquad (18)$$

where

$$(N_i, M_i^w, M_i^f) = \sum_{k=1}^{N}\int_{z_{k-1}}^{z_k} (1, z, f(z))\sigma_i^k dz, i = x, y, xy \qquad (19a)$$

$$Q_i = \sum_{k=1}^{N}\int_{z_{k-1}}^{z_k} f'(z)\sigma_i^k \, dz, i = xz, \ yz \tag{19b}$$

By substituting equation (13) into equation (19) and integrating across the thickness of the plate, the stress resultants can be linked to the strain through the following relations:

$$\begin{Bmatrix} N_x \\ N_y \\ N_{xy} \\ M_x^w \\ M_y^w \\ M_{xy}^w \\ M_x^f \\ M_y^f \\ M_{xy}^f \end{Bmatrix} = \begin{bmatrix} \begin{bmatrix} A_{11} & A_{12} & A_{16} \\ A_{12} & A_{22} & A_{26} \\ A_{16} & A_{26} & A_{66} \end{bmatrix} & \begin{bmatrix} B_{ij} \end{bmatrix} & \begin{bmatrix} C_{ij} \end{bmatrix} \\ \begin{bmatrix} B_{ij} \end{bmatrix} & \begin{bmatrix} D_{ij} \end{bmatrix} & \begin{bmatrix} E_{ij} \end{bmatrix} \\ \begin{bmatrix} C_{ij} \end{bmatrix} & \begin{bmatrix} E_{ij} \end{bmatrix} & \begin{bmatrix} F_{ij} \end{bmatrix} \end{bmatrix} \begin{Bmatrix} \begin{Bmatrix} u_{0,x} \\ v_{0,y} \\ u_{0,y}+v_{0,x} \end{Bmatrix} \\ \begin{Bmatrix} -w_{0,xx} \\ -w_{0,yy} \\ -2w_{0,xy} \end{Bmatrix} \\ \begin{Bmatrix} \phi_{x,x} \\ \phi_{y,y} \\ \phi_{x,y}+\phi_{y,x} \end{Bmatrix} \end{Bmatrix}; i,j=1,2,6 \tag{20a}$$

$$\begin{Bmatrix} Q_{yz} \\ Q_{xz} \end{Bmatrix} = \begin{bmatrix} H_{44} & H_{45} \\ H_{45} & H_{55} \end{bmatrix} \begin{Bmatrix} \gamma_{yz}^f \\ \gamma_{xz}^f \end{Bmatrix} \tag{20b}$$

where

$$\left(A_{ij}, B_{ij}, D_{ij}, C_{ij}, E_{ij}, F_{ij} \right) = \sum_{k=1}^{N}\int_{z_{k-1}}^{z_k} \overline{Q}_{ij}^k \left(1, z, z^2, f(z), zf(z), f^2(z) \right) dz; i,j=1,2,6 \tag{21a}$$

$$H_{ij} = \sum_{k=1}^{N}\int_{z_{k-1}}^{z_k} \overline{Q}_{ij}^k \left(f'(z) \right)^2 dz; i,j=4,5 \tag{21b}$$

The virtual potential energy of the external applied load is computed by:

$$\delta V = \int_V \left[N_x^0 w_{0,x}\delta w_{0,x} + N_y^0 w_{0,y}\delta w_{0,y} \right] dxdydz \tag{22}$$

where $N_x^0 = \gamma_x N_{cr}$ and $N_y^0 = \gamma_y N_{cr}$ are the in-plan compressive forces.

The expression for the kinetic energy of the mass system is as follows:

$$\delta T = \int_V \rho \left[\dot{u}\delta\dot{u} + \dot{v}\delta\dot{v} + \dot{w}\delta\dot{w} \right] dxdydz \tag{23}$$

$$\delta T = \int_A \begin{bmatrix} I_1\left(\dot{u}_0\delta\dot{u}_0 + \dot{v}_0\delta\dot{v}_0 + \dot{w}_0\delta\dot{w}_0\right) + \\[4pt] I_2\left(\dot{w}_{0,x}\delta\dot{u}_0 + \dot{w}_{0,y}\delta\dot{v}_0 + \dot{u}_0\delta\dot{w}_{0,x} + \dot{v}_0\delta\dot{w}_{0,y}\right) + \\[4pt] I_3\left(\dot{w}_{0,x}\delta\dot{w}_{0,x} + \dot{w}_{0,y}\delta\dot{w}_{0,y}\right) + \\[4pt] I_4\left(\dot{\phi}_x\delta\dot{u}_0 + \dot{u}_0\delta\dot{\phi}_x + \dot{\phi}_y\delta\dot{v}_0 + \dot{v}_0\delta\dot{\phi}_y\right) - \\[4pt] I_5\left(\dot{\phi}_x\delta\dot{w}_{0,x} + \dot{w}_{0,x}\delta\dot{\phi}_x + \dot{\phi}_y\delta\dot{w}_{0,y} + \dot{w}_{0,y}\delta\dot{\phi}_y\right) + \\[4pt] I_6\left(\dot{\phi}_x\delta\dot{\phi}_x + \dot{\phi}_y\delta\dot{\phi}_y\right) \end{bmatrix} dxdy \tag{24}$$

where

$$\left(I_1, I_2, I_3, I_4, I_5, I_6\right) = \sum_{k=1}^{N}\int_{z_{k-1}}^{z_k} \rho^k\left(1, z, z^2, f(z), zf(z), f^2(z)\right)dz \tag{25}$$

Substituting (18), (22) and (24) into (16) gives the equations of motion for the plate:

$$\delta u_0 : N_{x,x} + N_{xy,y} = I_1\ddot{u}_0 - I_2\ddot{w}_{0,x} + I_4\ddot{\phi}_x$$

$$\delta v_0 : N_{xy,x} + N_{y,y} = I_1\ddot{v}_0 - I_2\ddot{w}_{0,y} + I_4\ddot{\phi}_y$$

$$\delta w_0 : M^w_{x,xx} + 2M^w_{xy,xy} + M^w_{y,yy} + N^0_x w_{0,xx} + N^0_y w_{0,yy}$$

$$= I_1\ddot{w}_0 + I_2\left(\ddot{u}_{0,x} + \ddot{v}_{0,y}\right) - I_3\left(\ddot{w}_{0,xx} + \ddot{w}_{0,yy}\right) + I_5\left(\ddot{\phi}_{x,x} + \ddot{\phi}_{y,y}\right) \tag{26}$$

$$\delta\phi_x : M^f_{x,x} + M^f_{xy,y} - Q_{xz} = I_4\ddot{u}_0 - I_5\ddot{w}_{0,x} + I_6\ddot{\phi}_x$$

$$\delta\phi_y : M^f_{y,y} + M^f_{xy,x} - Q_{yz} = I_4\ddot{v}_0 - I_5\ddot{w}_{0,y} + I_6\ddot{\phi}_y$$

Analytical solutions

In the current study, the rectangular plates are taken to be simply supported at all edges. The exact solution of (26) can be derived analytically by applying the following boundary conditions:

$$v_0 = w_0 = \phi_y = N_x = M^w_x = M^f_x = 0 \ at \ x = 0, a$$

$$u_0 = w_0 = \phi_x = N_y = M^w_y = M^f_y = 0 \ at \ y = 0, b \tag{27}$$

The following displacement expansions are provided to derive the closed-form solutions of (26) and fulfill the simply supported boundary conditions given in (27), following Navier's approach:

1253

$$u_0(x,y,t) = \sum_{m=1}^{\infty}\sum_{n=1}^{\infty} U_{mn} e^{i\omega t} \cos(\alpha x)\sin(\beta y)$$

$$v_0(x,y,t) = \sum_{m=1}^{\infty}\sum_{n=1}^{\infty} V_{mn} e^{i\omega t} \sin(\alpha x)\cos(\beta y)$$

$$w_0(x,y,t) = \sum_{m=1}^{\infty}\sum_{n=1}^{\infty} W_{mn} e^{i\omega t} \sin(\alpha x)\sin(\beta y) \qquad (28)$$

$$\phi_x(x,y,t) = \sum_{m=1}^{\infty}\sum_{n=1}^{\infty} \Phi_{xmn} e^{i\omega t} \cos(\alpha x)\sin(\beta y)$$

$$\phi_y(x,y,t) = \sum_{m=1}^{\infty}\sum_{n=1}^{\infty} \Phi_{ymn} e^{i\omega t} \sin(\alpha x)\cos(\beta y)$$

where U_{mn}, V_{mn}, W_{mn}, Φ_{xmn} and Φ_{ymn} are arbitrary parameters that need to be determined. ω represents the eigen frequency linked to the (m,n) eigen mode. $\alpha = m\pi/a$ and $\beta = n\pi/b$.

By substituting equations (20) and (28) into equation (26), we can then derive the analytical solutions from the following equations

$$\left(\begin{bmatrix} s_{11} & s_{12} & s_{13} & s_{14} & s_{15} \\ s_{12} & s_{22} & s_{23} & s_{24} & s_{25} \\ s_{13} & s_{23} & s_{33} & s_{34} & s_{35} \\ s_{14} & s_{24} & s_{34} & s_{44} & s_{45} \\ s_{15} & s_{25} & s_{35} & s_{45} & s_{55} \end{bmatrix} - \omega^2 \begin{bmatrix} m_{11} & m_{12} & m_{13} & m_{14} & m_{15} \\ m_{12} & m_{22} & m_{23} & m_{24} & m_{25} \\ m_{13} & m_{23} & m_{33} & m_{34} & m_{35} \\ m_{14} & m_{24} & m_{34} & m_{44} & m_{45} \\ m_{15} & m_{25} & m_{35} & m_{45} & m_{55} \end{bmatrix} \right) = \begin{Bmatrix} 0 \\ 0 \\ 0 \\ 0 \\ 0 \end{Bmatrix} \qquad (29)$$

where

$$s_{11} = -A_{11}\alpha^2 - A_{66}\beta^2; s_{12} = -\alpha\beta(A_{12}+A_{66}); s_{13} = B_{11}\alpha^3 + B_{12}\alpha\beta^2 + 2B_{66}\alpha\beta^2;$$

$$s_{14} = -C_{11}\alpha^2 - C_{66}\beta^2; s_{15} = -\alpha\beta(C_{12}+C_{66}); s_{22} = -A_{22}\beta^2 - A_{66}\alpha^2;$$

$$s_{23} = B_{12}\alpha^2\beta + B_{22}\beta^3 + 2B_{66}\beta\alpha^2; s_{24} = s_{15}; s_{25} = -C_{22}\beta^2 - C_{66}\alpha^2;$$

$$s_{33} = -D_{11}\alpha^4 - 2(D_{12}+2D_{66})\alpha^2\beta^2 - D_{22}\beta^2 + N_x^0\alpha^2 + N_y^0\beta^2; \qquad (30a)$$

$$s_{34} = E_{11}\alpha^3 + E_{12}\alpha\beta^2 + 2E_{66}\alpha\beta^2; s_{35} = E_{12}\alpha^2\beta + E_{22}\beta^3 + 2E_{66}\beta\alpha^2;$$

$$s_{44} = -F_{11}\alpha^2 - F_{66}\beta^2 - H_{55}; s_{45} = -\alpha\beta(F_{12}+F_{66}); s_{55} = -F_{22}\beta^2 - F_{66}\alpha^2 - H_{44}$$

$$m_{11} = m_{22} = -I_1; m_{12} = m_{15} = m_{24} = m_{45} = 0; m_{13} = I_2\alpha;$$

$$m_{14} = m_{25} = -I_4; m_{23} = I_2\beta; m_{33} = -I_1 - I_3(\alpha^2 + \beta^2); \qquad (30b)$$

$$m_{34} = I_5\alpha; m_{35} = I_5\beta; m_{44} = m_{55} = -I_6$$

The numerical results in this study are presented using the subsequent dimensionless parameters:

$$\bar{N}_{cr} = \frac{N_{cr}a^2}{\pi^2 D_0}, D_0 = \frac{E^m h^3}{12\left[1-\left(v^m\right)^2\right]}, \bar{\omega} = \omega\frac{b^2}{h}\sqrt{\frac{\rho_m}{E_m}} \tag{31}$$

Results and the discussion

The material properties of the CNTRC layers utilized throughout this work are provided in Table 1. (10,10) armchair SWCNTs are selected as reinforcements, and Poly{(mphenylenevinylene)-co-[(2,5-dioctoxy-p-phenylene) vinylene]}, referred to as PmPV, as the matrix. G_{13}^{CNT} and G_{23}^{CNT} are assumed to be equal to G_{12}^{CNT}.

Table 1 – Characteristics of the CNTs and the matrix

		E_1 (GPa)	E_2 (GPa)	G_{12} (GPa)	ρ (kg/m³)	v_{12}
CNTs	(10,10) armchair SWCNT	5.6466x103	7.08x103	1.9445x103	1400	0.175
Matrix	PmPV	2.1	2.1	0.7358	1150	0.34

The efficiency parameters η_i for the CNTs are defined in Table 2. η_3 is assumed to be equal to η_2 (Zhu et al, 2012).

Table 2 – Efficiency parameters of the CNTs

V_{CNT}^*	η_1	η_2
0.11	0.149	0.934
0.14	0.150	0.941
0.17	0.149	1.381

Buckling analysis

It is worth mentioning that the FG-V distribution type is excluded from consideration in this section. This is due to the presence of stretching-bending coupling attribute in the FG-V layer, provoked by its asymmetry, causing deflections and bending moments when the plate experiences compressive loading.

As a first step, it is crucial to verify the accuracy and efficiency of the mathematical formulation presented in earlier sections for forecasting the buckling behavior of porous laminated FG-CNTRC plates. For this purpose, a comparison is conducted between the dimensionless critical buckling load $\overline{N}_{cr}$ of an FG-CNTRC plate obtained by the present method and those reported by Zhu et al. (2012) (HSDT), Wattanasakulpong & Chaikittiratana (2015) (TSDPT, SSDPT) and Guessas et al. (2018) (FSDT) based on various theories, as shown in Table 3. The results confirm the excellent agreement between the current results and those of previous studies.

Table 3 – Comparison of the dimensionless critical buckling load of FG-CNTRC square plates

b/h	V_{CNT}^*	Source	Uniaxial compressive load ($\gamma_x=-1;\gamma_y=0$)			Biaxial compressive load ($\gamma_x=-1;\gamma_y=-1$)		
			UD	FG-O	FG-X	UD	FG-O	FG-X
10	0.11	HSDT	20.6814	14.4990	24.2864	10.3407	7.2495	12.1432
		TSDPT	20.6814	14.4990	24.2864	10.3407	7.2495	12.1432
		SSDPT	20.7286	14.4515	24.3943	10.3643	7.2257	12.1972
		FSDT	20.5412	14.9792	23.9594	10.2706	7.4896	11.9797
		present	20.6814	14.4990	24.2864	10.3407	7.2495	12.1432
100	0.17	TSDPT	65.0043	35.1143	94.7137	32.5021	17.5572	47.3569
		SSDPT	65.0053	35.1126	94.7163	32.5026	17.5563	47.3581
		present	65.0043	35.1143	94.7137	32.5021	17.5572	47.3569

Table 4 presents the dimensionless critical buckling load of symmetric cross-ply laminated FG-CNTRC plate with and without porosity (P) under uniaxial and biaxial compressive loading. The results reveal that porosity exerts a significant influence on the critical buckling load, which decreases considerably with an increase in porosity. This decrease is attributed to the negative effect of porosity on the rigidity of the plate. Furthermore, It can be observed that the critical buckling load is high for the FG-X distribution type and low for the FG-O distribution type. In agreement with Lei et al. (2013), it is concluded that CNTs distributed near the top and bottom surfaces of each layer outperform those distributed closer to the mid-plane in enhancing the stiffness of the laminated FG-CNTRC plate. Additionally, regarding the effect of the number of layers on the critical buckling load, it is observed that increasing the number of layers leads to an increase in the critical buckling load.

Table 4 – Effect of porosity on the dimensionless critical buckling load of the porous cross-ply laminated FG-CNTRC square plate ($b/h=10$; $V_{CNT}^{*}=0.11$)

Lamination scheme	P	Uniaxial compressive load ($\gamma_x=-1$; $\gamma_y=0$)			Biaxial compressive load ($\gamma_x=-1$; $\gamma_y=-1$)		
		UD	FG-O	FG-X	UD	FG-O	FG-X
[0°/90°/0°]	0	21.7292	20.1795	23.3611	10.8646	10.0898	11.6806
	0.1	19.5563	18.1615	21.0250	9.7781	9.0808	10.5125
	0.2	17.3833	16.1436	18.6889	8.6917	8.0718	9.3445
[0°/90°/ 90°/0°]	0	23.6661	22.7649	24.6746	11.8331	11.3825	12.3373
	0.1	21.2995	20.4884	22.2072	10.6500	10.2442	11.1036
	0.2	18.9329	18.2119	19.7397	9.4665	9.1060	9.8699
[0°/90°/0°/ 90°/0°]	0	24.9562	24.4626	25.5669	12.4781	12.2313	12.7835
	0.1	22.4606	22.0164	23.0102	11.2303	11.0082	11.5051
	0.2	19.9649	19.5701	20.4535	9.9825	9.7850	10.2268
[0°/90°/0° /90°/0°/ 90°/0°]	0	25.8034	25.5837	26.1409	12.9017	12.7918	13.0705
	0.1	23.2231	23.0253	23.5268	11.6115	11.5127	11.7634
	0.2	20.6427	20.4669	20.9127	10.3214	10.2335	10.4564
[0°/90°/0°/ 90°/0°/90°/ 0°/90°/0°]	0	26.1425	26.0335	26.3688	13.0712	13.0168	13.1844
	0.1	23.5282	23.4302	23.7320	11.7641	11.7151	11.8660
	0.2	20.9140	20.8268	21.0951	10.4570	10.4134	10.5475

Table 5 – Dimensionless critical buckling load of the porous cross-ply laminated FG-CNTRC square plate for different CNTs volume fractions ($b/h=10$)

V_{CNT}^{*}	P	Uniaxial compressive load ($\gamma_x=-1$; $\gamma_y=0$)			Biaxial compressive load ($\gamma_x=-1$; $\gamma_y=-1$)		
		UD	FG-O	FG-X	UD	FG-O	FG-X
0.11	0	24.9562	24.4626	25.5669	12.4781	12.2313	12.7835
	0.1	22.4606	22.0164	23.0102	11.2303	11.0082	11.5051
	0.2	19.9649	19.5701	20.4535	9.9825	9.7850	10.2268
0.14	0	28.9296	28.3851	29.7241	14.4648	14.1925	14.8620
	0.1	26.0366	25.5466	26.7517	13.0183	12.7733	13.3758
	0.2	23.1437	22.7081	23.7793	11.5718	11.3540	11.8896
0.17	0	38.8356	38.2169	39.9517	19.4178	19.1084	19.9758
	0.1	34.9521	34.3952	35.9565	17.4760	17.1976	17.9783
	0.2	31.0685	30.5735	31.9613	15.5343	15.2868	15.9807

The dimensionless critical buckling load of porous symmetric cross-ply [0°/90°/0°/90°/0°] laminated FG-CNTRC plates for various CNTs volume fractions and different porosity volume fraction are presented in Table 5. The findings indicate that that as the volume fraction of CNTs increases, the critical buckling load rises accordingly. This is attributed to the fact that the stiffness of the laminated FG-CNTRC plate further increases by adding an extra amount of CNTs volume fraction. However, this increase becomes less significant in the presence of porosity.

Figure 2 provides the variation of the dimensionless critical buckling load of porous symmetric angle-ply laminated FG-CNTRC plates [θ°/-θ°/θ°/-θ°/θ°] in relation to the variation of the CNTs orientation angle θ for different porosity volume fractions. Upon inspection of Figure 2, it is evident that the critical buckling load increases as θ changes from 0° to 45°, then decreases as θ changes from 45° to 90°, with the critical buckling loads being symmetric to θ = 45°. The latter presents the largest values of critical buckling load for all reinforcement types and in both uniaxial and biaxial compressive loading. Consistent with previous findings, plates with porosity exhibit low resistance against buckling compared to plates without porosity.
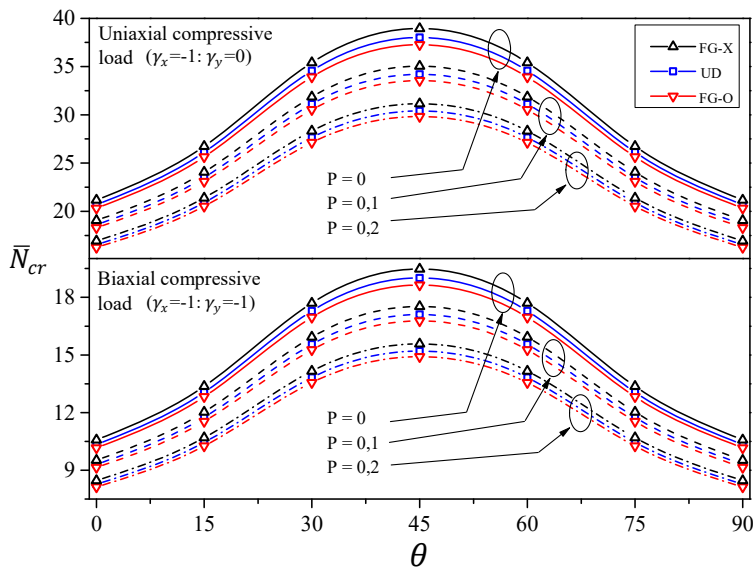

Figure 2 – Dimensionless critical buckling load of the porous angle-ply laminated FG-CNTRC square plate ($b/h=10$; $V^*_{CNT}=0.11$)

Free vibration analysis

For free vibration analysis, numerical validation is also performed. The present method is compared with that of Huang et al. (2017) for the free vibration of anti-symmetrically laminated FG-CNTRC plates in the absence of porosity, and the results show good agreement, as illustrated in Table 6. Table 6 lists the dimensionless fundamental frequency $\bar{\omega}$ for varying patterns of the CNTs distribution, the number of layers, the CNTs volume fraction V_{CNT}^* and the width-to-thickness ratio b/h. The small variation in the lower b/h ratios is attributed to the model proposed by Huang et al. (2017), which is a four-variable FSDT.

Table 6 – Comparison of dimensionless fundamental frequencies of FG-CNTRC anti-symmetric cross-ply laminated square plates

	Source	$\dfrac{b}{h}$	[0°/90°/0°/90°]			[0°/90°/0°/90°/0°/90°/0°/90°]		
			V_{CNT}^*					
			0.11	0.14	0.17	0.11	0.14	0.17
UD	Present	10	14.405	15.546	17.840	15.161	16.344	18.779
		20	16.776	18.500	20.707	17.866	19.711	22.049
		50	17.696	19.701	21.810	18.943	21.122	23.340
	Huang et al. (2017)	10	14.640	15.832	18.124	15.338	16.555	18.993
		20	16.872	18.624	20.820	17.944	19.811	22.142
		50	17.714	19.726	21.831	18.958	21.142	23.358
FG-V	Present	10	14.299	15.444	17.737	15.150	16.348	18.799
		20	16.621	18.330	20.529	17.838	19.687	22.032
		50	17.518	19.498	21.597	18.906	21.081	23.303
	Huang et al. (2017)	10	14.518	15.717	17.993	15.302	16.534	18.975
		20	16.683	18.424	20.596	17.881	19.754	22.078
		50	17.495	19.484	21.565	18.883	21.065	23.271
FG-O	Present	10	14.166	15.293	17.574	15.116	16.308	18.757
		20	16.496	18.190	20.375	17.808	19.652	21.995
		50	17.396	19.362	21.448	18.878	21.050	23.269
	Huang et al. (2017)	10	14.450	15.649	17.909	15.288	16.519	18.957
		20	16.581	18.314	20.470	17.859	19.729	22.049
		50	17.378	19.354	21.421	18.856	21.036	23.238
FG-X	Present	10	14.668	15.852	18.202	15.238	16.445	18.910
		20	17.071	18.839	21.092	17.944	19.806	22.165
		50	18.003	20.054	22.204	19.019	21.211	23.445
	Huang et al. (2017)	10	14.794	16.007	18.344	15.363	16.596	19.052
		20	17.099	18.888	21.120	17.977	19.859	22.197
		50	17.975	20.032	22.165	18.995	21.193	23.411

Table 7 presents the three lowest dimensionless frequencies for symmetric cross-ply porous laminated FG-CNTRC plates with different porosity volume fractions. Upon comparing the results, it can be observed that the frequencies show weak dependence on porosity, with the frequency decreasing very slightly with the increase of porosity. The same observation can be made from Figures 4 and 5. This can be attributed to the fact that the effect of porosity on the density is as important as its effect on the rigidity of the plate. Additionally, the FG-X distribution type exhibits the largest frequencies compared to the UD, FG-V and FG-O for every mode. It is also evident that the effect of the number of layers is manifested in the increase of the frequency as the number of layers increases.

Table 7 – Effect of porosity on the dimensionless frequency of the porous cross-ply laminated FG-CNTRC square plate ($b/h = 10$; $V_{CNT}^* = 0.11$)

	P	[0°/90°/0°]				[0°/90°/0°/90°/0°]			
		UD	FG-V	FG-O	FG-X	UD	FG-V	FG-O	FG-X
1st Mode	0	13.8958	13.6781	13.3887	14.4106	14.9041	14.9219	14.7553	15.0858
	0.1	13.8779	13.6604	13.3713	14.3919	14.8848	14.9026	14.7362	15.0662
	0.2	13.8555	13.6383	13.3498	14.3687	14.8608	14.8786	14.7124	15.0419
2nd Mode	0	20.8993	20.0286	19.2837	22.2633	26.8626	26.9065	26.5834	27.2181
	0.1	20.8722	20.0027	19.2588	22.2344	26.8278	26.8716	26.5490	27.1828
	0.2	20.8386	19.9704	19.2277	22.1985	26.7845	26.8283	26.5062	27.1390
3rd Mode	0	33.2531	32.8548	32.0150	34.4913	33.7417	33.8055	33.3006	34.2971
	0.1	33.2100	32.8123	31.9736	34.4466	33.6980	33.7617	33.2575	34.2527
	0.2	33.1564	32.7594	31.9220	34.3909	33.6436	33.7072	33.2038	34.1974
		[0°/90°/0°/90°/0°/90°/0°]				[0°/90°/0°/90°/0°/90°/0°/90°/0°]			
1st Mode	0	15.1576	15.1748	15.0925	15.2564	15.2578	15.2748	15.2257	15.3237
	0.1	15.1379	15.1552	15.0729	15.2367	15.2381	15.2551	15.2060	15.3039
	0.2	15.1135	15.1307	15.0486	15.2121	15.2135	15.2304	15.1814	15.2792
2nd Mode	0	28.5479	28.5952	28.4286	28.7590	29.4004	29.4495	29.3453	29.5527
	0.1	28.5109	28.5581	28.3918	28.7217	29.3624	29.4114	29.3073	29.5144
	0.2	28.4649	28.5121	28.3460	28.6754	29.3150	29.3639	29.2600	29.4668
3rd Mode	0	33.6851	33.7463	33.4966	33.9928	33.4966	33.5563	33.4098	33.7017
	0.1	33.6415	33.7026	33.4532	33.9488	33.4533	33.5128	33.3665	33.6580
	0.2	33.5872	33.6482	33.3992	33.8940	33.3993	33.4588	33.3127	33.6037

Figure 3 depicts the effect of porosity on the amplitude of a four layered unidirectional [0°/0°/0°/0°] porous laminated FG-CNTRC plate in

different modes of vibration. It is clear that the results are almost identical in terms of values for all modes of vibration.

Thus, we can state that porosity has a negligible effect on the amplitude of the plate.

This result further confirms the weakening effect of porosity on the free vibration response of the laminated FG-CNTRC plate.
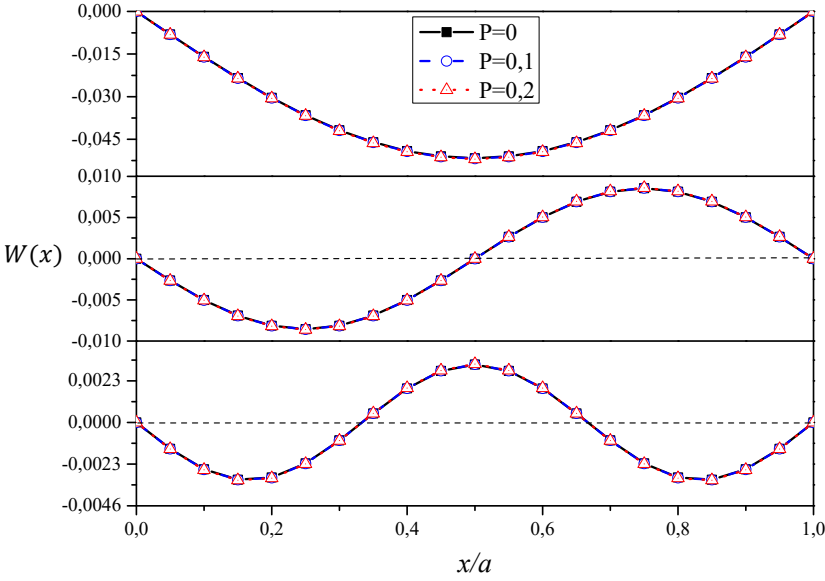

Figure 3 – Amplitude of the unidirectional porous laminated FG-CNTRC square plate
$(b/h = 10 ; V_{CNT}^{*} = 0.11)$

The variation in the dimensionless fundamental frequency of porous anti-symmetric cross-ply laminated FG-CNTRC plates [0°/90°/0°/90°] with respect to the variation of the CNTs volume fraction and the porosity volume fraction is depicted in Figure 4.

It is noticeable that the increase in the CNTs volume fraction leads to a significant increase in the fundamental frequency for all CNTs distribution types.
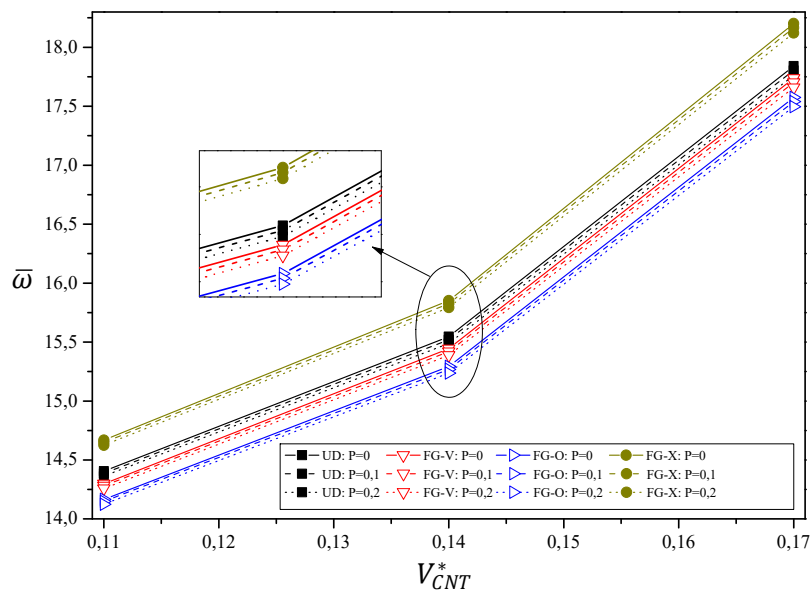
Figure 4 – Variation of the dimensionless frequency of the four layered porous anti-symmetric cross-ply laminated FG-CNTRC square plate in the function of the variation of the CNTs volume fraction ($b/h=10$)

Figure 5 presents the variation of the dimensionless fundamental frequency of the anti-symmetric angle-ply laminated FG-CNTRC plate [θ°/-θ°/θ°/-θ°] in relation to the variation of the CNTs orientation angle (θ) for different porosity volume fractions.

The fundamental frequency increases as θ changes from 0° to 45°, then decreases as θ changes from 45° to 90°, in which the fundamental frequencies are symmetric to θ = 45°. This last mentioned value (θ =45°) presents the largest values of fundamental frequency for all cases.

According to the above investigations, it can be noticed that porosity has a low impact on the frequency of laminated FG-CNTRC plates compared to the effects of the other parameters.
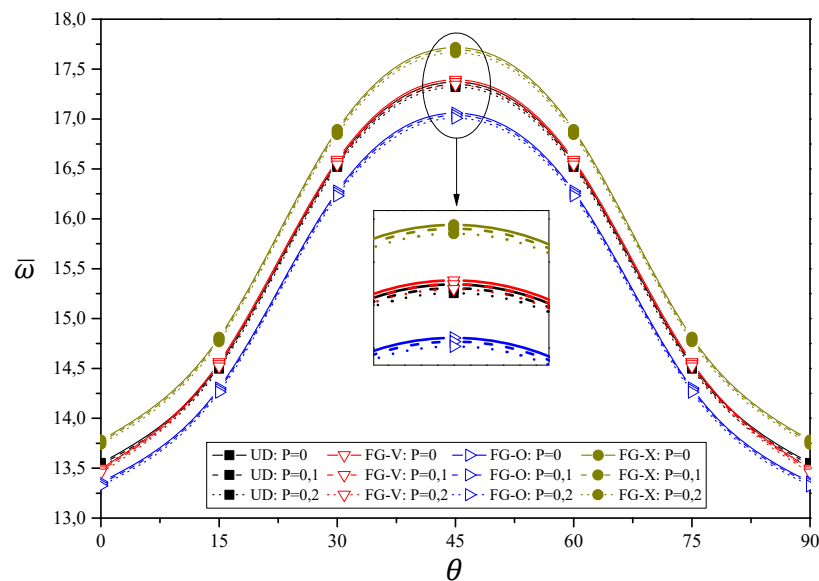
Figure 5 – Dimensionless frequency of the porous angle-ply laminated FG-CNTRC square plate ($b/h = 10$; $V_{CNT}^{*} = 0.11$)

The minimal influence of porosity on the plate's amplitude and frequency across various vibration modes suggests the resilient nature of the laminated FG-CNTRC plate structure to porosity effects. While porosity typically alters material stiffness, the specific arrangement of composite layers in this case seems to counteract such effects. Consistently uniform results imply effective mitigation of porosity-induced changes in amplitude and frequency by the plate's design and material composition. This highlights the robustness of the laminated FG-CNTRC plate against porosity-induced variations in vibrational characteristics, further confirming its weakened free vibration response due to porosity.

Conclusion

In this paper, the buckling and free vibration of laminated FG-CNTRC plates in the presence of porosity are analytically examined. A mathematical model based on a five-unknown HSDT is developed. The assumption is made that the laminates consist of layers that are perfectly bonded, with carbon nanotubes (CNTs) distributed throughout the thickness of each layer, accounting for different types of FG distributions.

The effective material properties are determined using the extended rule of mixture considering an upper limit of the impact of porosity. The accuracy of the present formulation has been validated, and detailed parametric studies have been conducted to examine the effects of several parameters on the critical buckling load and natural frequency of porous laminated FG-CNTRC plates. Some typical conclusions are noted:

- In terms of porosity, it is found that porosity has a considerable negative effect on the critical buckling load.
- Porosity has a weak effect on the free vibration characteristics.
- Increasing the CNTs volume fraction enhances plate rigidity.The enhancement becomes less significant in the presence of porosity.
- For the CNTs distribution type, it is derived that reinforcements distributed near the top and bottom surfaces of the layer outperform those distributed closer to the mid-plane in enhancing the stiffness of the plate.
- The number of layers significantly impacts the responses to free vibration and buckling. The critical buckling load and natural frequency rise in proportion to the increase in the number of layers.
- The lamination angle significantly influences both the critical buckling load and natural frequency. Because of the axial symmetry of the laminated square plate orientations at 45°, any changes in these properties are also symmetrical.

In future works, it would be beneficial to explore the influence of environmental conditions on laminated FG-CNTRC plates' mechanical properties and durability. Additionally, investigating dynamic responses under various loading conditions and conducting experimental validation could enhance reliability. Exploring advanced manufacturing techniques and novel materials could also improve performance and expand application possibilities.

References

Alimoradzadeh, M., Heidari, H., Tornabene, F. & Dimitri, R. 2023. Thermo-Mechanical Buckling and Non-Linear Free Oscillation of Functionally Graded Fiber-Reinforced Composite Laminated (FG-FRCL) Beams. *Applied Sciences*, 13(8), art.number:4904. Available at: https://doi.org/10.3390/app13084904.

Arani, A.G., Kiani, F. & Afshari, H. 2021. Free and forced vibration analysis of laminated functionally graded CNT-reinforced composite cylindrical panels. *Journal of Sandwich Structures & Materials*, 23(1), pp.255-278. Available at: https://doi.org/10.1177/1099636219830787.

Chiker, Y., Bachene, M., Attaf, B., Hafaifa, A. & Guemana, M. 2023. Uncertainty influence of nanofiller dispersibilities on the free vibration behavior of multi-layered functionally graded carbon nanotube-reinforced composite laminated plates. *Acta Mechanica*, 234(4), pp.1687-1711. Available at: https://doi.org/10.1007/s00707-022-03438-6.

Ciriscioli, P.R., Springer, G.S. & Lee, W.I. 1991. An Expert System for Autoclave Curing of Composites. J*ournal of Composite Materials*, 25(12), pp.1542-1587. Available at: https://doi.org/10.1177/002199839102501201.

Daikh, A.A., Belarbi, M.-O., Salami, S.J., Ladmek, M., Belkacem, A., Houari, M.S.A., Ahmed, H.M. & Eltaher, M.A. 2023. A three-unknown refined shear beam model for the bending of randomly oriented FG-CNT/fiber-reinforced composite laminated beams rested on a new variable elastic foundation. *Acta Mechanica*, 234(10), pp.5171-5186. Available at: https://doi.org/10.1007/s00707-023-03657-5.

Fu, T., Chen, Z., Yu, H., Wang, Z. & Liu, X. 2019. Mechanical behavior of laminated functionally graded carbon nanotube reinforced composite plates resting on elastic foundations in thermal environments. *Journal of Composite Materials*, 53(9), pp.1159-1179. Available at: https://doi.org/10.1177/0021998318796170.

Guessas, H., Zidour, M., Meradjah, M. & Tounsi, A. 2018. The critical buckling load of reinforced nanocomposite porous plates. *Structural Engineering and Mechanics*, 67(2), pp.115-123. Available at: https://doi.org/10.12989/sem.2018.67.2.115.

Hagstrand, P.-O., Bonjour, F. & Månson, J.-A.E. 2005. The influence of void content on the structural flexural performance of unidirectional glass fibre reinforced polypropylene composites. *Composites Part A: Applied Science and Manufacturing*, 36(5), pp.705-714. Available at: https://doi.org/10.1016/j.compositesa.2004.03.007.

Hayashi, T. & Takahashi, J. 2017. Influence of void content on the flexural fracture behaviour of carbon fiber reinforced polypropylene. *Journal of Composite Materials*, 51(29), pp.4067-4078. Available at: https://doi.org/10.1177/0021998317698215.

Hernández, S., Sket, F., Molina-Aldareguı´a, J.M., González, C. & LLorca, J. 2011. Effect of curing cycle on void distribution and interlaminar shear strength in polymer-matrix composites. *Composites Science and Technology*, 71(10), pp.1331-1341. Available at: https://doi.org/10.1177/0021998317698215.

Huang, B., Guo, Y., Wang, J., Du, J., Qian, Z., Ma, T. & Yi, L. 2017. Bending and free vibration analyses of antisymmetrically laminated carbon nanotube-reinforced functionally graded plates. *Journal of Composite Materials*, 51(22), pp.3111-3125. Available at: https://doi.org/10.1177/0021998316685165.

Kirchhoff, G. 1850. Über das Gleichgewicht und die Bewegung einer elastischen Scheibe. *Journal für die reine und angewandte Mathematik (Crelles Journal)*, 1850(40), pp.51-88. Available at: https://doi.org/10.1515/crll.1850.40.51.

Kwon, H., Bradbury, C.R. & Leparoux, M. 2011. Fabrication of Functionally Graded Carbon Nanotube-Reinforced Aluminum Matrix Composite. *Advanced Engineering Materials*, 13(4), pp.325-329. Available at: https://doi.org/10.1002/adem.201000251.

Lee, J., Kim, J. & Hyeon, T. 2006. Recent Progress in the Synthesis of Porous Carbon Materials. *Advanced Materials*, 18(16), pp.2073-2094. Available at: https://doi.org/10.1002/adma.200501576.

Lei, Z.X., Liew, K.M. & Yu, J.L. 2013. Buckling analysis of functionally graded carbon nanotube-reinforced composite plates using the element-free kp-Ritz method. *Composite Structures*, 98, pp.160-168. Available at: https://doi.org/10.1016/j.compstruct.2012.11.006.

Lei, Z.X., Zhang, L.W. & Liew, K.M. 2018. Modeling large amplitude vibration of matrix cracked hybrid laminated plates containing CNTR-FG layers. *Applied Mathematical Modelling*, 55, pp.33-48. Available at: https://doi.org/10.1016/j.apm.2017.10.032.

Liew, K.M., Lei, Z.X. & Zhang, L.W. 2015. Mechanical analysis of functionally graded carbon nanotube reinforced composites: A review. *Composite Structures*, 120, pp.90-97. Available at: https://doi.org/10.1016/j.compstruct.2014.09.041.

Ma, R. & Jin, Q. 2023. Free Vibration Analysis of Functionally Graded Graphene-Reinforced Composite-Laminated Plates. *Journal of Aerospace Engineering*, 36(3), art.ID:04023016. Available at: https://doi.org/10.1061/JAEEEZ.ASENG-4657.

Madsen, B. & Lilholt, H. 2003. Physical and mechanical properties of unidirectional plant fibre composites—an evaluation of the influence of porosity. *Eco-Composites*, 63(9), pp.1265-1272. Available at: https://doi.org/10.1016/S0266-3538(03)00097-6.

Madsen, B., Thygesen, A. & Lilholt, H. 2009. Plant fibre composites – porosity and stiffness. *Composites Science and Technology*, 69(7), pp.1057-1069. Available at: https://doi.org/10.1016/j.compscitech.2009.01.016.

Malekzadeh, P. & Shojaee, M. 2013. Buckling analysis of quadrilateral laminated plates with carbon nanotubes reinforced composite layers. *Thin-Walled Structures*, 71, pp.108-118. Available at: https://doi.org/10.1016/j.tws.2013.05.008.

Mantari, J.L., Oktem, A.S. & Guedes Soares, C. 2012. A new trigonometric shear deformation theory for isotropic, laminated composite and sandwich plates. *International Journal of Solids and Structures*, 49(1), pp.43-53. Available at: https://doi.org/10.1016/j.ijsolstr.2011.09.008.

Medani, M., Benahmed, A., Zidour, M., Heireche, H. & Tounsi, A. 2019. Static and dynamic behavior of (FG-CNT) reinforced porous sandwich plate using energy principle. *Steel and Composite Structures*, 32(5), pp.595-610. Available at: https://doi.org/10.12989/scs.2019.32.5.595.

Mehdikhani, M., Gorbatikh, L., Verpoest, I. & Lomov, S.V. 2019. Voids in fiber-reinforced polymer composites: A review on their formation, characteristics, and effects on mechanical performance. *Journal of Composite Materials*, 53(12), pp.1579-1669. Available at: https://doi.org/10.1177/0021998318772152.

Mindlin, R.D. 1951. Influence of rotatory inertia and shear on flexural motions of isotropic, elastic plates. *Journal of Applied Mechanics*, 18(1), pp.31-38. Available at: https://doi.org/10.1115/1.4010217.

Phani, K.K. & Niyogi, S.K. 1987. Young's modulus of porous brittle solids. *Journal of Materials Science*, 22(1), pp.257-263. Available at: https://doi.org/10.1007/BF01160581.

Reddy, J.N. 1984. A Simple Higher-Order Theory for Laminated Composite Plates. *Journal of Applied Mechanics*, 51(4), pp.745-752. Available at: https://doi.org/10.1115/1.3167719.

Sayyad, A.S. & Ghugal, Y.M. 2015. On the free vibration analysis of laminated composite and sandwich plates: A review of recent literature with some numerical results. *Composite Structures*, 129, pp.177-201. Available at: https://doi.org/10.1016/j.compstruct.2015.04.007.

Shen, H.S. 2009. Nonlinear bending of functionally graded carbon nanotube-reinforced composite plates in thermal environments. *Composite Structures,* 91(1), pp.9-19. Available at: https://doi.org/10.1016/j.compstruct.2009.04.026.

Shimpi, R.P., Arya, H. & Naik, N.K. 2003. A Higher Order Displacement Model for the Plate Analysis. *Journal of Reinforced Plastics and Composites*, 22(18), pp.1667-1688. Available at: https://doi.org/10.1177/073168403027618.

Stamopoulos, A.G., Tserpes, K.I., Průcha, P. & Vavřík, D. 2016. Evaluation of porosity effects on the mechanical properties of carbon fiber-reinforced plastic unidirectional laminates by X-ray computed tomography and mechanical testing. *Journal of Composite Materials*, 50, pp.2087-2098. Available at: https://doi.org/10.1077/0021998315602049.

Thai, H.-T. & Choi, D.-H. 2011. A refined plate theory for functionally graded plates resting on elastic foundation. *Composites Science and Technology*, 71(16), pp.1850-1858. Available at: https://doi.org/10.1016/j.compscitech.2011.08.016.

Thai, H.-T. & Vo, T.P. 2013. A new sinusoidal shear deformation theory for bending, buckling, and vibration of functionally graded plates. *Applied Mathematical Modelling*, 37(5), pp.3269–3281. Available at: https://doi.org/10.1016/j.apm.2012.08.008.

Tran, H.Q., Vu, V.T., Tran, M.T. & Nguyen-Tri, P. 2020. A new four-variable refined plate theory for static analysis of smart laminated functionally graded carbon nanotube reinforced composite plates. *Mechanics of Materials*, 142, art.number:103294. Available at: https://doi.org/10.1016/j.mechmat.2019.103294.

Wattanasakulpong, N. & Chaikittiratana, A. 2015. Exact solutions for static and dynamic analyses of carbon nanotube-reinforced composite plates with Pasternak elastic foundation. *Applied Mathematical Modelling*, 39(18), pp.5459-5472. Available at: https://doi.org/10.1016/j.apm.2014.12.058.

Zhang, L.W. & Selim, B.A. 2017. Vibration analysis of CNT-reinforced thick laminated composite plates based on Reddy's higher-order shear deformation theory. *Composite Structures*, 160, pp.689-705. Available at: https://doi.org/10.1016/j.compstruct.2016.10.102.

Zhu, P., Lei, Z.X. & Liew, K.M. 2012. Static and free vibration analyses of carbon nanotube-reinforced composite plates using finite element method with first order shear deformation plate theory. *Composite Structures*, 94(4), pp.1450-1460. Available at: https://doi.org/10.1016/j.compstruct.2011.11.010.

Investigación analítica sobre el pandeo y la vibración libre de placas laminadas porosas FG-CNTRC

Tahir Ghazoul[a], **autor de correspondencia,** *Mohamed Atif* Benatta[a],
Abdelwahhab Khatir[b], *Youcef* Beldjelili[a],
Baghdad Krour[a], *Mohamed* Bachir Bouiadjra[a]

[a] Universidad de Djillali Liabes, Laboratorio de Estructuras y Materiales
    Avanzados en Ingeniería Civil y Obras Públicas,
    Sidi Bel Abbes, República Argelina Democrática y Popular,

[b] Universidad Politécnica de Marche, Sección Estructural DICEA,
    Ancona, República Italiana

CAMPO: mecánica, materiales
TIPO DE ARTÍCULO: artículo científico original

Resumen:

Introducción/objetivo: El objetivo de este estudio es examinar el comportamiento de pandeo y vibración libre de las placas compuestas laminadas, reforzadas con nanotubos de carbono cuando se tienen en cuenta varias fuentes de incertidumbre, siendo el enfoque principal la existencia de porosidad.

Métodos: Se desarrolla un modelo de placa laminada porosa utilizando la teoría de la deformación por corte de alto orden. Se investigan diferentes configuraciones de nanotubos de carbono de pared simple alineados y funcionalmente graduados en todo el espesor de cada capa. Las propiedades efectivas de los materiales se evalúan a través de la regla extendida de mezcla mientras se considera un límite superior para el efecto de la porosidad. Las ecuaciones que rigen se derivan y resuelven utilizando el principio de trabajo virtual y el enfoque de Navier. La validez de la formulación actual se confirma comparando nuestros resultados con los datos existentes de fuentes bibliográficas. Se investiga en detalle el impacto de numerosos parámetros como la porosidad, la fracción de volumen de nanotubos de carbono, los tipos de distribución de refuerzo, el esquema de laminación y el número de capas en las respuestas de pandeo y vibración libre.

Resultados: Un hallazgo clave de este estudio es la reducción significativa en la resistencia al pandeo de las placas laminadas FG-CNTRC debido a la porosidad, en contraste con el impacto menor en la respuesta de vibración libre.

Conclusión: Los resultados de este artículo enfatizan el papel crítico de la porosidad en la integridad estructural y brindan nuevos conocimientos sobre el comportamiento de los materiales compuestos avanzados.

Palabras claves: pandeo, vibración libre, placa compuesta laminada, porosidad, material funcionalmente graduado, nanotubos de carbono.

Аналитическое исследование изгиба и свободной вибрации пористых слоистых пластин FG-CNTRC

Тахир Газул[а], **корреспондент**, *Мухаммед Атиф* Бената[а],
Абделвахаб Катир[б], *Йусуф* Белджелили[а],
Багдад Кроур[а], *Мухаммед* Башир Буjажера[а]

[а] Университет Джиллали Лиабес, Лаборатория конструкций и
  современных материалов в гражданском строительстве
  и общественных работах,
  г. Сиди-Бель-Аббес, Алжирская Народно-Демократическая Республика

[б] Политехнический университет Марке, структурное подразделение
  DICEA, г. Анкона, Итальянская Республика

Резюме:

Введение/цель: Целью данного исследования является изучение изгиба и свободной вибрации многослойных композитных пластин, армированных углеродными нанотрубками, при учете различных источников неопределенности с акцентом на наличие пористости.

Методы: Модель многослойной пористой пластины разработана с применением теории сдвиговой деформации высокого порядка. Исследовались различные конфигурации функционально упорядоченных выровненных одностенных углеродных нанотрубок по толщине каждого слоя. Эффективные свойства материалов оцениваются с помощью расширенного правила смешивания с учетом верхнего предела пористости. Управляющие уравнения получены и решены с помощью принципа виртуальной работы и подхода Навье. Обоснованность этой формулировки подтверждается сравнением результатов с данными из существующих научных источников. Подробно исследовано влияние многочисленных параметров, таких как пористость, объемная доля углеродных нанотрубок, виды распределения армирования, схема ламинирования и количество слоев на изгибе и реакция на свободную вибрацию.

Результаты: Ключевым выводом данного исследования является значительное снижение сопротивления

ламинированных пластин FG-CNTRC на изгиб из-за их пористости, в отличии от незначительного влияния на отклик на свободную вибрацию.

Выводы: Результаты данной статьи подчеркивают критическую роль пористости в целостности структуры и дают новое представление о поведении современных композитных материалов.

Ключевые слова: изгиб, свободная вибрация, многослойная композитная пластина, пористость, функционально распределенный материал, углеродные нанотрубки.

Аналитичко испитивање порозних ламинираних плоча од функционално градираних композита ојачаних угљеничним наноцевима (FG-CNTRC) на извијање и слободне вибрације

Тахир Газул[а], **аутор за преписку,** *Мухамед Атиф* Бената[а],
Абделвахаб Катир[б], *Јусуф* Белџелили[а],
Багдад Кроур[а], *Мухамед* Башир Бујажера[а]

[а] Универзитет Ђилали Лиабес, Лабораторија за
   напредне конструкције и материјале у грађевинарству и јавним
   радовима, Сиди Бел Абес, Народна Демократска Република Алжир

[б] Политехнички универзитет Марке, Структурни одсек DICEA,
   Анкона, Република Италија

ОБЛАСТ: механика, материјали
КАТЕГОРИЈА (ТИП) ЧЛАНКА: оригинални научни рад

Сажетак:

Увод/циљ: Циљ ове студије јесте да испита понашање ламинираних композитних плоча ојачаних угљеничним наноцевима при извијању и слободним вибрацијама када се узимају у обзир различити извори несигурности и када је фокус на постојању порозности.

Методе: Модел порозне ламиниране плоче развијен је помоћу смицајне деформационе теорије вишег реда. Испитане су различите конфигурације функционално градираних угљеничних наноцеви с једноструким зидом, поређаних целом дебљином сваког слоја. Ефективна својства материјала процењена су кроз прошрено правило о смешама, узимајући у обзир горњу границу ефекта порозности. Водеће једначине изведене су и решене помоћу принципа виртуалног рада и Навијеровог приступа. Валидност наведене формулације потврђена је поређењем добијених резултата са подацима из постојеће литературе. Детаљно је испитан утицај бројних параметара попут порозности, запреминског удела угљеничних наноцеви, типова дистрибуције

ојачања, шеме ламинације, као и броја слојева на извијање и одговора на слободне вибрације.

Резултати: Кључни налаз ове студије јесте да је знатно смањена отпорност на извијање ламинираних FG-CNTRC плоча услед порозности, за разлику од минорног утицаја на одговор на слободне вибрације.

Закључак: Резултати овог рада истичу критичну улогу порозности у интегритету структуре и пружају нове увиде у понашање напредних композитних материјала.

Кључне речи: извијање, слободна вибрација, ламинирана композитна плоча, порозност, функционално градиран материјал, угљеничне наноцеви.